Sensors & Transducers, Vol. 203, Issue 8, August 2016, pp. 8-15

Sensors & Transducers

http://www.sensorsportal.com

Development of Unified Fabrication Process and Testing of MEMS Based Comb and Crab Type Capacitive Accelerometers for Navigational Applications

R. K. Bhan, Shaveta, Imran, Ramjay Pal, Shankar Dutta and Isha Yadav
Solid State Physics Laboratory, DRDO, Lucknow Road, Timarpur, Delhi, India – 110054
E-mail: bhan_rk2003@yahoo.com

Received: 18 July 2016 /Accepted: 18 August 2016 /Published: 31 August 2016

Abstract: MEMS based accelerometers have already penetrated defense programs including navigation control in addition to their usual deployment in automotive, consumer and industrial markets because of their improved reliability, accuracy and excellent price performance. This paper discussed about the fabrication and testing of single axis capacitive accelerometer structures based on change in area (comb-type) and change in gap (Crab type) sensing principles. The accelerometers are designed for ±30 g acceleration range. A common fabrication process flow is designed for the fabrication of both types of accelerometers that are fabricated by using a three mask dissolved wafer process (DWP). Both the accelerometers showed a scale factor sensitivity of >60 mV/g at ±1 g flip test. Vibration and sensitivity testing at higher frequency was conducted on shaker table using a half sine wave shock (HSWS) of 2 ms. Using HSWS test, a sensitivity in the range of ~60 mV/g was obtained for both comb or crab type structures in the 0-30 g range. It can be further tuned upto 100 mV/g by increasing the gain of the capacitance Read Out Integrated Circuit (ROIC). However, performance of the comb type of accelerometers gets affected in – 30 g to – 0 g range due to deep boron diffusion induced residual stress. The crab accelerometers showed almost linear (nonlinearity: <3 % FS) behavior in the whole ±30 g range. Other tests like bias stability, bandwidth, bias temperature coefficient etc. indicate that devices are fully functional. All these observations validate our design and unified process.

Keywords: Microccelerometer, MEMS, Capacitive accelerometer, Comb type, Crab type.

1. Introduction

Silicon micro-electro-mechanical system (MEMS) technology based accelerometers have replaced the established, expensive and high-end fragile electromechanical devices. The MEMS based accelerometers offer improved performance at lower cost, lower power consumption, smaller size, high reliability and reproducibility. They have already penetrated defense programs including navigation control due to their reliability, accuracy and excellent bias stability performances.

In MEMS technology, different sensing principles, like piezoresistive, piezoelectric and capacitive, are utilized to sense acceleration. Out of them, capacitive sensing mechanism is preferred due to high sensitivity, low noise, low temperature sensitivity and low power dissipation characteristics [1-3]. This accelerometer can be designed based on either change in gap or change in area approach. Both the approaches have their advantages and disadvantages. Whereas, the change in gap type accelerometers can be fabricated using variety of process recipes [4], the change in area type has not many process recipe variants available

[5]. Here, we propose and show that both types of accelerometers mentioned above can indeed be fabricated using a common fabrication process recipe for the same targeted specifications. Whereas, in comb type accelerometers, it is the number of fingers that is varied and in crab type it the area of the proof mass to achieve the targeted capacitance. Both the accelerometer structures are designed for ±30 g dynamic range and particularly targeted for navigational application. Both the accelerometer structures have MEMS based fixed capacitors, so that the accelerometers can be operated in differential capacitance mode. The change in capacitance due to applied acceleration is converted into electrical signal (voltage) by using off the shelf Read Out Integrated Circuit (ROIC) ASIC MS 3110 [6]. Vibration testing of both comb and crab type structures is done on shaker system.

2. Accelerometer Structures

Schematics of the comb type and crab type accelerometer structures are shown in Fig. 1(a) and Fig. 1(b) respectively.

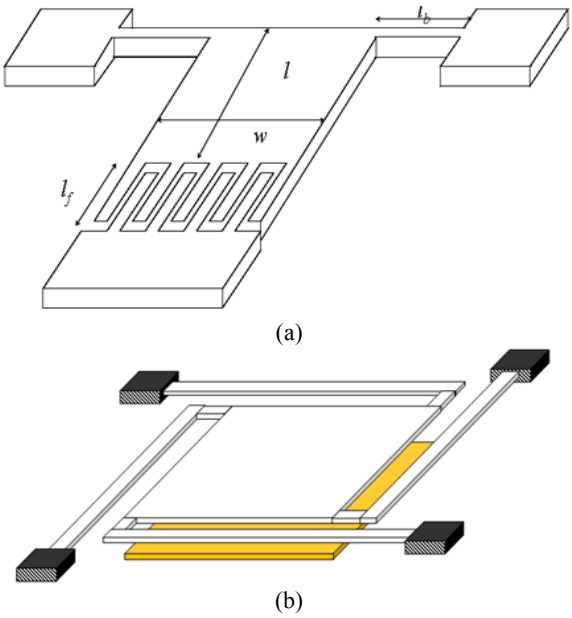

Fig. 1. Isometric schematic of (a) comb type, and (b) crab type microaccelerometer structures.

The comb structure consists of 12 µm thick boron-doped silicon proof mass suspended by two narrow 12 µm × 5 µm torsion beams over 8 µm glass cavity. Large number of movable fingers are attached with the proof mass. Each finger has the dimension of 500 µm × 12 µm × 5 µm with a interfinger gap of 4 µm. There are also a number of fixed fingers in between the comb fingers. Together they form a comb like structure with inter finger gap of 4 µm. Fig. 1(b) shows crab type accelerometer structure that consists of 1000 µm × 1000 µm × 12 µm proof mass and is suspended over 5 µm glass cavity suspended by four L-shaped beams (10 µm × 25 µm × 12 µm) which are anchored to substrate.

3. Fabrication Process

In this work, a unified process flow was developed for fabrication of both the accelerometer structures. The accelerometer structures were realized using a common three mask dissolved wafer process (DWP). Fig. 2 shows the fabrication process flow used for realization of the accelerometer structures. Thickness of the accelerometer structures was defined by heavy boron diffusion of concentration > 5×10^{19} atoms/ cc upto a depth of ~ 12 µm as shown in step (b) of Fig. 2. The boron diffusion experiments were carried out at 1175 °C in a mixture of nitrogen and oxygen atmosphere. Details of the diffusion experiment can be found out elsewhere [7]. This heavily boron doping will act as etch stop during the final stages of DWP process in chemical etchant. Thereafter, the comb and crab type accelerometer structures were patterned by deep reactive ion etching (DRIE) recipe (Bosch process) using photoresist (Shipley S1818) as masking layer (Mask 1) as shown in step (c) of Fig. 2.

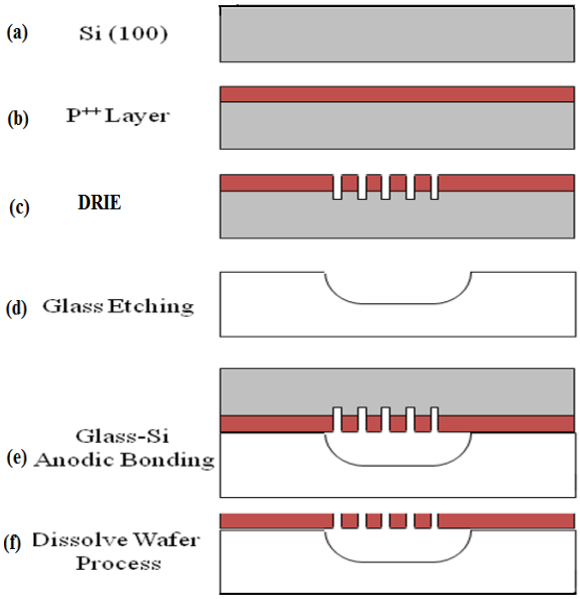

Fig. 2. (a) Si 100, (b) boron diffusion, (c) DRIE of Comb or Crab Type, (d) Glass cavity etching, (e) Glass – Si anodic bonding, (f) Dissolved Wafer Process (DWP).

In parallel, cavities were formed in Pyrex 7740 glass wafers using wet chemical etching in HF and HNO_3 acidic mixture (7:3) as shown in step 4 of Fig. 2. Here, Cr-Au layer was used for the masking purpose (Mask 2). The depths of the cavity were kept ~8 µm and ~5 µm for the comb and crab type accelerometer structures respectively. Then, Ti-Au

layer was coated on the glass substrate after removing the Cr-Au layer. Thereafter, electrical contact lines and contact pads of the Ti-Au layer were patterned (Mask 3).

The patterned glass and silicon wafers were then bonded (anodic bonding) together as shown in step (e) of Fig. 2. Finally, the whole silicon wafer was dissolved in aqueous alkaline solutions (KOH and EDP), leaving behind the boron doped structural layer of accelerometer structures.

Using the said unified fabrication process, both the structures were successfully fabricated. Fig. 3 shows the SEM images of suspended comb and crab type accelerometer structures.

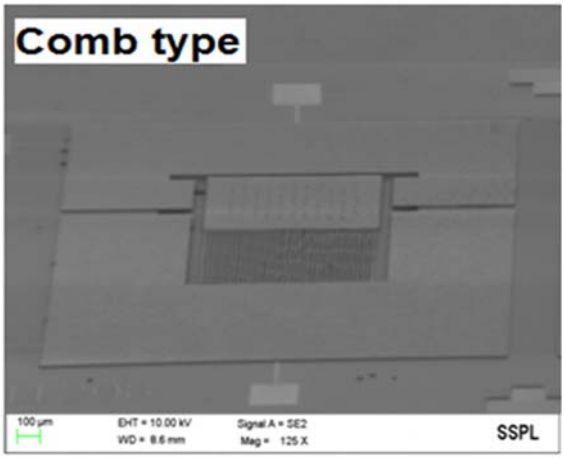

(a)

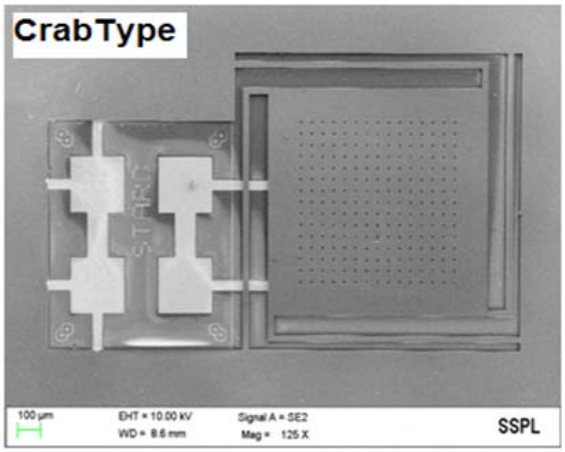

(b)

Fig. 3. SEM images of (a) comb and (b) crab type accelerometer structures.

4. Testing of Comb and Crab Type Accelerometers

After fabricating the comb and crab type accelerometer structures using unified fabrication process flow, the devices were tested both at wafer level as well as after hybrid packaging using off the shelf MS 3110 ROIC [6] for converting capacitance change to analog voltage output.

4.1. Wafer Level Capacitance Voltage (C-V) Measurements

The rest capacitance of fabricated accelerometer structures was measured at the wafer level (before chip dicing) using Kithley Semiconductor Parametric Analyzer 4200 model. The zero bias capacitance values confirm about the release of the structure, however, if it is shorted due to collapse or due to unwanted foreign particles, there will be unexpected capacitance/inductance values.

The accelerometers were also tested at different DC applied voltage (±5 V) with superimposing AC signal. Further, crab type structures exhibited shallow U-type C-V characteristics. Fig. 4 shows the C-V characteristics of the crab structures. Most of the measured devices showed shallow U-type CV characteristics indicating that the structures are properly released and the devices are responding to change in actuation voltage as per our theoretical predictions and experimental results reported earlier [8].

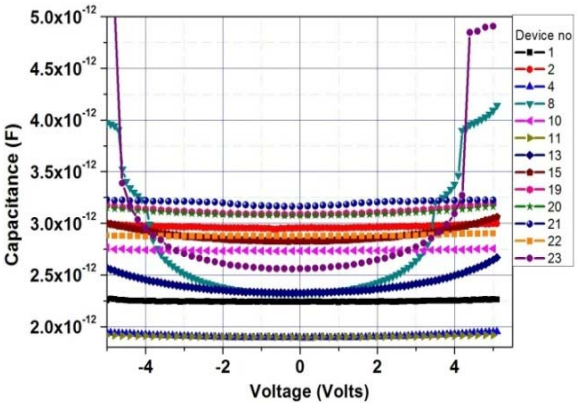

Fig. 4. Results of C-V measurements for 13 crab accelerometer devices.

4.2. Packaging

After qualifying the accelerometers structures by C-V measurements, they are packaged along with the ROIC chip. Fig. 5 shows the assembly (without final top sealing lid) of the complete prototype along with its evaluation board that is used for electrical and Shaker table testing. A temperature sensor as close as possible has also been mounted on the PCB. This is utilized for estimating the temperature coefficient of bias stability of the accelerometer. Further there are some de-coupling capacitors also on the board. The ROIC is programmable and the sensitivity can be increased by using its programmable capability. It can even be used to reduce the mismatch between reference and movable capacitor.

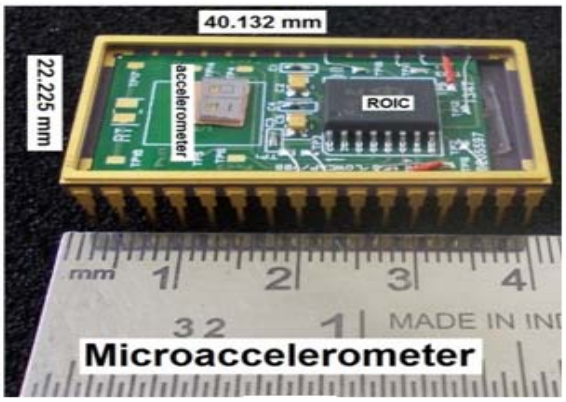

(a)

(b)

Fig. 5. The prototype of the packaged microaccelerometer in (a) 32 pin package (b) with evaluation board and low noise output connector.

4.3. Vibration Testing

After packaging with the ROIC chip, both the accelerometers were tested on Bruel & Kjear LDS shaker system (model no v201-PA 25E). Testing of accelerometer was done by using classic shock module of the shaker software. The output of the accelerometers were measured in ±30 g range at 250 Hz. Measurement results of comb and crab type accelerometers in unregulated temperature condition are shown in Fig. 6 (a) and Fig. 6 (b). The sensitivity of the different comb type structures were tuned in the range of 55 – 87 mV/g for 0 – 30 g range. The output of the comb accelerometer was found to be almost linear in the 0 – 30 g range (Fig. 6(a)). However, the performance (sensitivity) of the comb accelerometers was seriously hindered in -30 g to 0 g range. It happened primarily due to presence of large boron diffusion induced residual stress [7, 9-10]. This problem was discussed in details in our earlier publication [10].

Fig. 6(b) shows the typical output of the crab type accelerometer measured on the shaker table in ±30 g range. The sensitivity of the crab accelerometer was found to be 75 mV/g in ±30 g range with <1.2 % nonlinearity (full scale).

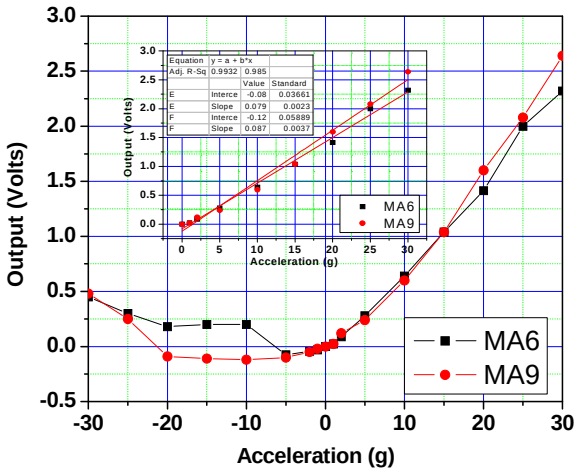

Fig. 6 (a). Typical response of comb type accelerometers on shaker table in ±30 g range.

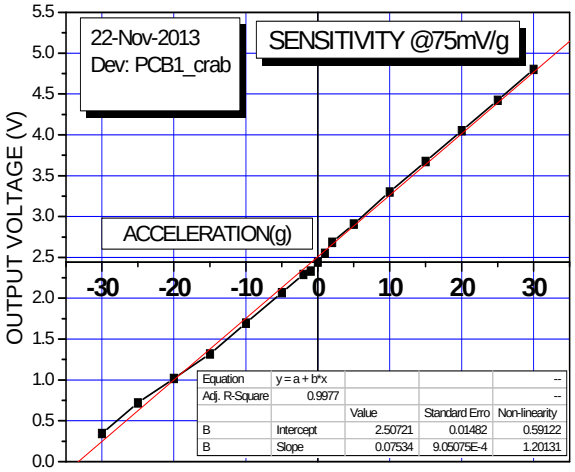

Fig. 6 (b). Typical response of crab type accelerometers on shaker table in ±30 g range.

Fig. 7 shows comparison of the output of comb and crab type accelerometers in 0 – 30 g range.

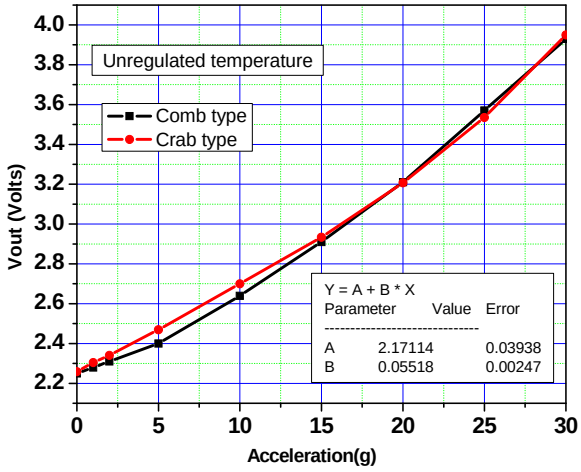

Fig. 7. Comparison of output of comb and crab type accelerometers in 0 - 30 g range.

As expected, the comb type accelerometer showed better linearity than the crab accelerometer in 0 – 30 g range. But the problem of the comb accelerometers in – 30 g to 0 g range seriously restricted its possibility to use it in the ±30 g range for navigational applications. Hence forward, we are reporting the other testing results of only crab type structures for navigational applications.

4.4. Flip Test

To check the response of gravitational acceleration on the crab accelerometers a ±1 g flip test is conducted initially. In the flip test, the accelerometer showed an output voltage change of about 0.1914 V over 2.25 V null conditions. To further see the effect of vertical inclination angle on the accelerometer, the accelerometer outputs are studied on an inclinometer from Bosch Lamb having a resolution of 0.1 degrees. Fig. 8(a) shows the accelerometer output voltage at different inclination angles in ±90° range. As expected, the output followed a sine wave variation. From the inclination data, the output voltage of the accelerometer is observed in ±1 g range as shown in Fig. 8(b). The studied crab accelerometer showed a typical linear behavior with a scale factor sensitivity of 95 mV/g. From the inclinometer measurement, the cross-axis sensitivity of the accelerometer is found to be ~ 2 %.

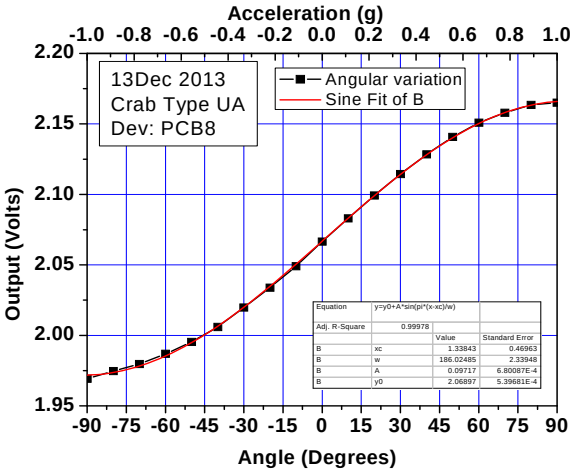

Fig. 8 (a). Typical output voltage versus angle measured on an inclinometer using a prototype of the packaged microaccelerometer.

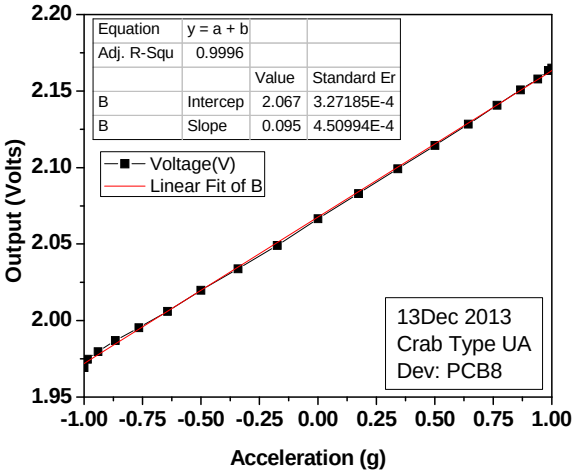

Fig. 8 (b). Typical output voltage versus 'g' using a prototype of the packaged microaccelerometer. The measured data converted to ±1 g showing sensitivity of 95 mV/ g.

4.5. Centrifuge Measurements

Centrifuge testing is one of the important testing steps to qualify accelerometers for quantative acceleration testing. In this test, the sensor is mounted on a centrifuge in such a way that the sensing axis is in radial direction. The sensor is suitably rotated at different speeds to obtain upto 30 g acceleration in steps. The output measured at different accelerations applied from 0 to 30 g. The measurement is repeated while mounting the sensor in opposite direction (by flipping) and thus recording the data from 0 to -30 g. The results are plotted in Fig. 9. It may be seen that the sensitivity i.e. slope is varying from 94 to 106 mV/g for the three crab devices (MA2, MA3 and MA4). The slope has been estimated from the linear fit of the data.

4.6. Frequency Response - Bandwidth Measurements

Fig. 10 shows typical frequency response of crab accelerometer in comparison with commercial piezoelectric accelerometer which known to have better frequency response than the capacitive one.

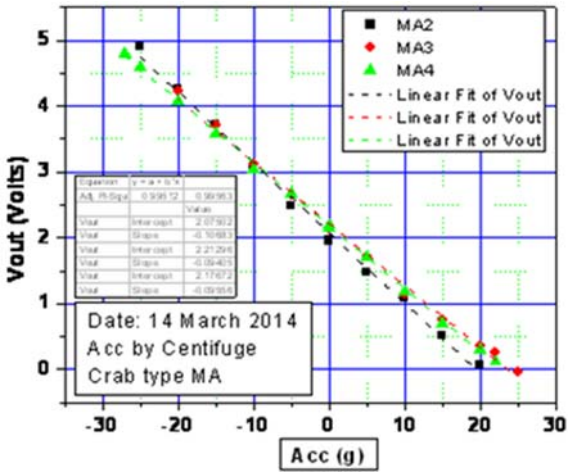

Fig. 9. Typical output of Crab type accelerometer for -30 to +30 g range showing the sensitivity of 94 to 106 mV/ g. in response +/- 30g acceleration applied by a centrifuge machine. The slope has been estimated from the linear fit of data for all the three devices.

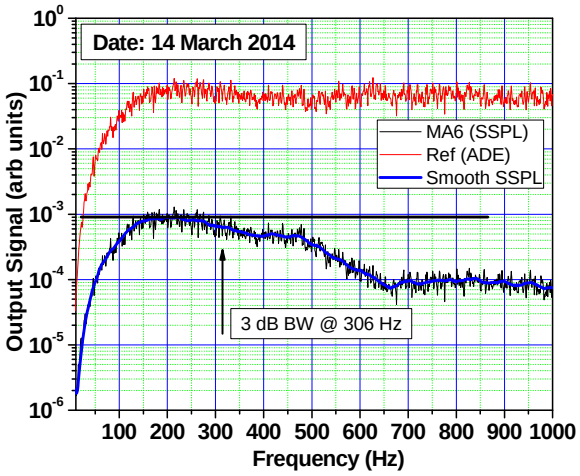

Fig. 10. Typical output of Crab type accelerometer on a Shaker table for 0 to 1 kHz full Sine Wave at 1 g condition.

The frequency response was measured using a shaker table operating at a fixed acceleration of 1 g. The crab accelerometer showed 3 dB cutoff frequency at 306 Hz. This compares well to our design value of >250 Hz assuming no holes in the membrane. Our structure still represents an over damping case. The un-stability of the shaker table in the frequency response from 0-150 Hz could be easily seen from the reference detectors response. This prevented us from extracting the actual expected flat response in the low frequency range.

4.7. Bias Stability over Time

MEMS accelerometers are key components in a great variety of applications and, particularly, in navigation systems. Non-idealities such as bias, scale factors, cross coupling etc. affect the output of this sensor, leading, in general, to prohibitive errors. On the other hand, these coefficients are often time-varying, which renders off-line calibration less effective. One such coefficient that usually varies greatly over time and between power-on is the bias. Hence it is important to measure it and control it. The typical short term bias stability of our crab type accelerometer is shown in Fig. 11(a) and is ±5 mg within 10 min. The typical long term bias stability of our crab type accelerometer is shown in Fig. 11(b) and is measured for three days. It may be noted that a p-p variation of within 1 mV corresponding to about ±5 mg has been obtained upto 1000 minutes.

4.8. Bias Temperature Coefficient

The typical bias temperature coefficient of our crab type accelerometer in the range of -22 to +75 ºC has been measured and is linear as expected (Fig. 12). It is estimated to be about 0.048 % in the full dynamic range for this temperature. This data is useful for implementing on line temperature correction to the output of the accelerometer.

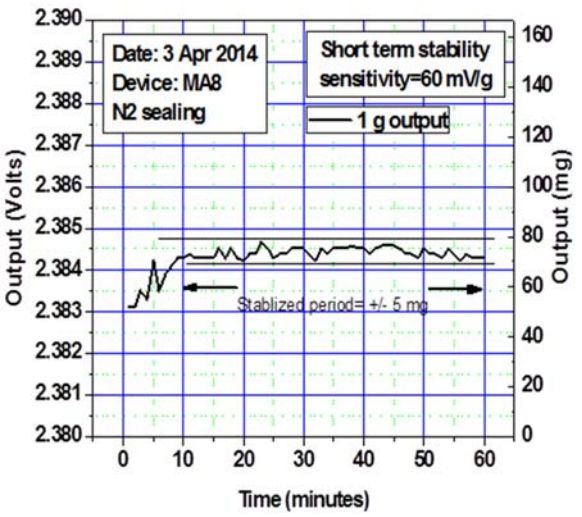

Fig. 11(a). Typical short term steady state output bias stability of crab accelerometer at 1 g condition.

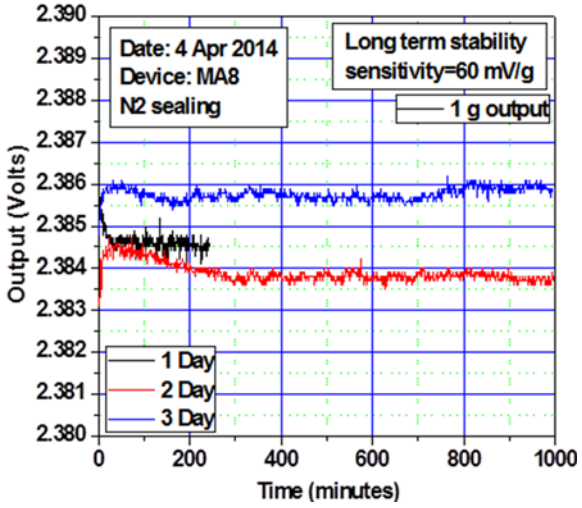

Fig. 11(b). Typical long term steady state output bias stability of crab accelerometer at 1 g condition.

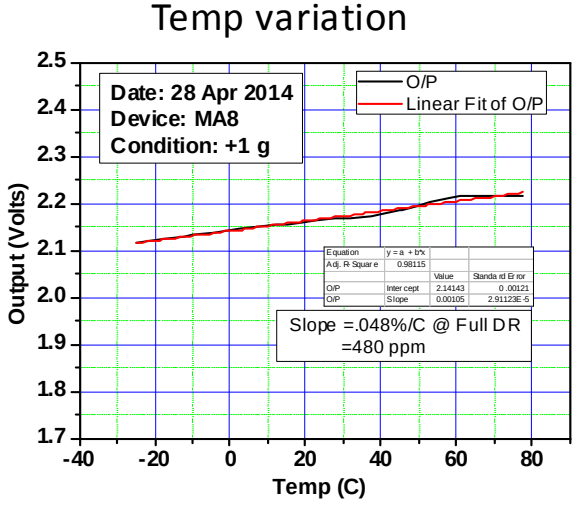

Fig. 12. Typical variation of output of accelerometer as a function of temperature at 1 g.

4.9. Noise

This is measured by monitoring the output @ at +1 g as a function of time in steady state condition. This measurement requires a quiet room with temperature regulation. Typical output of this measurement is shown in Fig. 13.

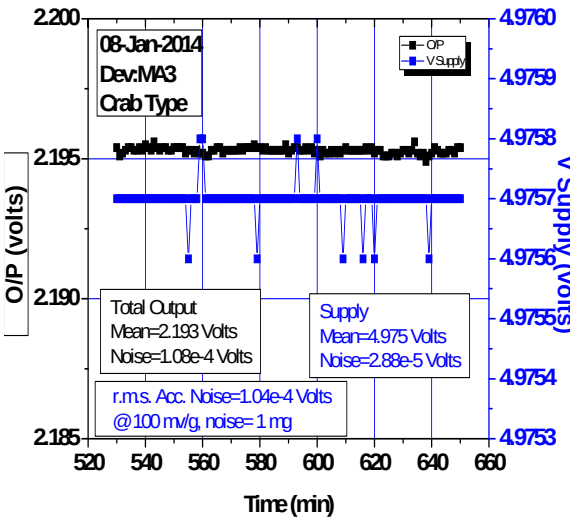

Fig. 13. Noise measurements using the stabilized 1 g output.

The noise in this case is calculated by:

$$n_t^2 = n_{supply}^2 + n_{acc}^2, \quad (1)$$

which is 1.04×10^{-4} r.m.s. volts. Using the conversion factor of 100 mV/g it amounts to full band rms noise of about 1 mg being added by accelerometer, if supply noise is controlled to within 50 micro volts. This noise can converted into volts/ √Hz by diving the number by sqrt of bandwidth i.e. about 17 in our case. Hence we have 0.0588 mg/√Hz.

The in band noise can be further reduced by incorporating low pass filters on the evaluation board.

4.10. Misalignment Error in Sensing Axis

The misalignment error in sensing axis of accelerometers should be minimal so that they can imply minimum inaccuracy in navigational applications. This is very crucial for high speed missiles and rockets. This error may arise from various misalignments or dimensional non-uniformities due to fabrication process limitations as well as integration issues during packaging. The misalignment errors due to the process variation and integration issues in z-axis crab accelerometers in our case are tabulated in Table 1.

Table 1. Estimation of misalignment errors of z-axis in accelerometer.

Item	Material	Shape	Dimensions		Thickness (min)	Thickness (max)	Diff (um)	Angle Radians
			Length (µm)	Width (µm)	(µm)	(µm)	(µm)	Milli radians
Evaluation Board (PCB)	FR4	Rectangle	50200	1575	1575	1725	150.000	2.9880
Socket		Rectangle	40132	5400	5400	5600	200.000	4.9835
Package base	Ceramic	Rectangle	40132	940	940	1092	152.000	3.7875
Epoxy	Epotek	Rectangle	40000	45	45	55	10.000	0.2500
Glass substrate	SiO_2	Rectangle	8400	699	699	701	2.0000	0.2381
Silicon	Si	Rectangle	8400	11	11	12	1.0000	0.1190
Total								12.3662

It may be seen from this table that there will be inherent non-parallelism in each layer used in mounting the accelerometer starting from silicon, glass, epoxy etc. Based on the actual measured data of non-parallelism in each layer a maximum misalignment error can be calculated. If it is assumed that all misalignments keep on adding in one direction, we get the maximum error as 12.36 milli radians. However, in practice it is expected that this error will be lower because all the layers will not be misaligned in one direction.

In our previous communication [11], we presented a new improved analytical approach based on differential and reciprocal differential of data of tilt measurement for determining the axis misalignment error i.e. the extent to which the accelerometers true sensitive axis deviates from being perfectly orthogonal to the accelerometers reference mounting surface when mounted to flat surface. Majority of manufacturers term this specification as "input axis misalignment". In our case, estimates from Table 1 agree reasonably well with the actual measured data as reported by us elsewhere [11].

5. Conclusions

Comb and crab type accelerometers are developed at SSPL using a common fabrication process based on dissolve wafer process. We have validated the proposed unified process by fabricating the actual prototypes and verifying the proof of concept. Reasonable sensitivity and linearity is obtained using the proposed processes.

Acknowledgements

The authors would like to thank Director, Solid State Physics Laboratory for his continuous support and for the permission to publish this work. Help from other colleagues of SEM group is also acknowledged.

References

[1]. G. Krishnan, C. U. Kshirsagar, G. K. Ananthasuresh, N. Bhat, Micromachined High-resolution Accelerometers, in *Journal of the Indian Institute of Science*, Vol. 87, No. 3, Jul.–Sep. 2007, pp. 333-361.

[2]. A. Selvakumar, A High-Sensitivity - Axis Capacitive Silicon Microaccelerometer with a Torsional Suspension, *Journal of Micromechanical Systems*, Vol. 7, No. 2, June 1998, pp. 192-200.

[3]. T. Tsuchiya, H. Funabashi, A z-axis Differential Capacitive SOI Accelerometer with Vertical Comb Electrodes, *Sensors & Actuator A*, Vol. 116, No. 3, 2004, pp. 378-383.

[4]. S. Dutta, R. Pal, R Chatterjee, Fabrication Challenges for Realization of Wet Etching Based Comb Type Capacitive Microaccelerometer Structure, *Sensors & Transducers*, Vol. 111, Issue 12, December 2009, pp. 18-24.

[5]. C. P. Hsu, M. C. Yip, W. Fan, Implementation of a gap-closing differential capacitive sensing Z-axis accelerometer on an SOI wafer, J. Micromech. Microeng., Vol. 19, No. 7, 2009.

[6]. Operation manual of MS3110 Universal Capacitive Readout IC, *Irvine Sensors Corporation.*

[7]. S. Dutta, A. Pandey, G. Saxena, R. Raman, A. Dhaul, R. Pal, R. Chatterjee, Characterization deep boron diffused p^{++} silicon layer, *J. Mater. Sci: Mater. Electron.*, Vol. 23, No. 8, 2012, pp. 1569-1574.

[8]. R. K. Bhan, Shaveta, A. Panchal, Y. Parmar, C. Sharma, R. Pal, S. Dutta, Determination of Multiple Spring Constants, Gaps and Pull Down Voltages in MEMS CRAB type Microaccelerometer using near Pull Down Capacitance Voltage Measurements, *Sensors & Transducers*, Vol. 192, Issue 9, September 2015, pp 44-52.

[9]. S. Dutta, G. Saxena, Shaveta, K. Jindal, R. Pal, V. Gupta, R. Chatterjee, Comparison of residual stress in deep boron diffused silicon (100), (110) and (111) wafers, *Mater. Lett.*, Vol. 100, 2013, pp. 44-46.

[10]. S. Dutta, Shaveta, Md. Imran, R. Pal, R. K. Bhan, Diffusion induced residual stress in comb-type microaccelerometer structure, *J. Mater. Sci: Mater. Electron.*, Vol. 25, Issue 9, 2014, pp. 3828-3832.

[11]. R. K. Bhan, Shaveta, Imran, Ramjai Pal, S. Dutta, An improved analytical approach for estimation of misalignment error of sensing axis in MEMS accelerometers using simple tilt measurements, *Sensors & Transducers*, Vol. 189, Issue 6, June 2015, pp. 128-136.